Shear-induced microstructure distortion and its relaxation for colloids very close to the critical point

Jan K. G. Dhont and Igor Bodnár
Van 't Hoff Laboratory for Physical and Colloid Chemistry, Debye Research Institute, Utrecht University, Padualaan 8, 3584 CH Utrecht, The Netherlands
(Received 10 April 1998)

Light scattering experiments on a stationary sheared colloidal system very close to the gas-liquid critical point, beyond the mean-field region, show that there is a pronounced shear-induced distortion of the structure factor in directions perpendicular to the flow direction for very small shear rates. This is contrary to what is found in the mean-field region, further away from the critical point, where the structure in these directions is unaffected. Light scattering experiments are presented for a colloid-polymer mixture and possible origins for this unexpected effect are discussed. After cessation of the shear flow we find an unusual relaxation phenomenon where the scattered intensity develops a ringlike structure, implying that there is an optimum relaxation rate at some intermediate wave vector. A theoretical explanation for this phenomenon is given, which shows that the scattering ring is the result of the interplay between a driving force and a rate limiting diffusion process. The phenomena that are observed experimentally are extensively compared to theoretical predictions. The necessary theoretical background is discussed in some detail. [S1063-651X(98)13810-2]

PACS number(s): 82.70.Dd, 82.20.Mj, 83.50.Ax, 64.60.Ht

I. INTRODUCTION

On approach of the gas-liquid critical point, the extent of spatial correlations between the (colloidal) particles increases without bound. The spatial extent of these correlations is measured by the correlation length, which thus diverges at the critical point. The effect of shear flow on these critical, long-range correlations is significant already for small shear rates, resulting in a highly anisotropic microstructure and thus giving rise to highly anisotropic scattering patterns.

Such a strong anisotropy of the scattered intensity of light is found by, e.g., Beysens and co-workers [1,2] in critical binary mixtures of fluids. They observe a strong anisotropy with respect to the flow direction. The experimental findings are interpreted in terms of the dimensionless parameter $\dot{\gamma}\tau_c$, with $\dot{\gamma}$ the shear rate and τ_c the relaxation time for critical fluctuations. This dimensionless number is the shear rate in units of the reciprocal relevant time scale τ_c. An essential ingredient in their data interpretation is the shear-induced shift of the critical temperature.

The effect of shear flow on critical fluctuations in low- and high-molecular-weight polymer blends has been studied by Nakatani *et al.* [3] and Hobbie *et al.* [4–6] by means of small-angle neutron scattering and dynamic light scattering. For the low molecular blends no anisotropy is found in the experimentally probed scattering angle range (there might be anisotropic scattering for smaller scattering angles, outside the experimental range). The isotropic scattering patters for the blends under stationary shear flow are fitted to Ornstein-Zernike equilibrium forms with a shear-rate-dependent correlation length. The shear rate dependence of the correlation length is attributed to the shear-flow-induced shift of the critical point, as predicted by Onuki, Yamazaki, and Kawasaki [7]. For the high-molecular-weight polymer blends, however, a strong anisotropy is observed, except in directions perpendicular to the flow direction, where the structure factor retains its equilibrium form. The wave vector k_c where the structure factor begins to deviate from its equilibrium form is found to be proportional to $\dot{\gamma}^{1/3}$, in accordance with predictions of Onuki, Yamazaki, and Kawasaki [7]. The relevance of the wave vector k_c is that $2\pi/k_c$ is the longest distances over which correlations are still unaffected by the applied shear flow.

In Sec. II we shall consider the role of the shear-induced shift of the critical point in the case of colloidal systems, as well as the shear-rate dependence of k_c and the relevance of the dimensionless parameter $\dot{\gamma}\tau_c$.

Only few experimental results are available on the relaxation of critical correlations after cessation of shear flow. Beysens, Gbadamassi, and Moncef-Bouanz [2] describe a relaxation experiment on a binary fluid mixture at one single scattering angle and observed single exponential relaxation with time. Relaxation experiments in polymer systems are reported by Wu, Pine, and Dixon [8], Dixon, Pine, and Wu [9], and van Egmond, Werner, and Fuller [10]. They find shear-flow-enhanced structures, leading to an *increase* of the turbidity. These effects are the result of strong entanglement and are fundamentally different from the phenomena discussed in the present paper. In binary liquids and in systems of rigid, spherical colloids the turbidity is found to sharply *decrease* on applying shear flow [2,11]. This sharp decrease of the turbidity is the result of strong reduction of microstructural order, contrary to the polymer systems in Refs. 8–10, where entanglement leads to enhanced microstructural order on applying shear flow.

In the present paper we report on shear-induced microstructural anisotropy and the relaxation of these anisotropic structures after cessation of the shear flow in a system of spherical colloids exhibiting a gas-liquid critical point. The relaxation phenomena are also discussed, in less detail, in Ref. [12]. As far as the structures under stationary shear flow are concerned, we shall focus on the difference in response

 © 1998 The American Physical Society

between systems in the mean-field region, away from the critical point, and systems very close to the critical point. In Sec. II the necessary theoretical background is given. This section contains all the ingredients necessary to understand and interpret the experimental findings. Section III gives the experimental details and results and Sec. IV is a summary and conclusion.

The flow field considered in the present paper is in the x direction, its gradient is in the y direction, and the z direction corresponds to the vorticity direction. The first component k_1 of the scattering vector $\mathbf{k}$ is thus its component along the flow direction, k_2 is its component along the gradient direction, and k_3 is along the vorticity direction. The experimental results presented in this paper relate to the flow-vorticity plane, where k_2 is practically zero.

II. THEORETICAL BACKGROUND

Notable theoretical approaches to describing stationary shear flow effects on microstructure are due to Onuki, Yamazaki, and Kawasaki [7,13], Schwarzl and Hess [14], Ronis [15], and Wagner and Russel [16]. The theoretical approach discussed in the following subsections is taken from Refs. [17,18], which specifically deal with colloidal systems near the critical point.

A. Shear-induced distortions under stationary shear flow

The dimensionless number that measures the amount of distortion of microstructure extending over distances r is the Péclet number $\dot\gamma r^2/2D$, where $\dot\gamma$ is the shear rate and D is the diffusion coefficient relevant for relaxation of microstructures of extent r. When the Péclet number is less than 1, the effects of shear on microstructures of extent r are small, while for Péclet numbers larger than 1 there is a significant distortion. As it will turn out, there are two length scales of interest in the vicinity of the critical point: the range R_V of the pair-interaction potential, which is of the order of the size of the core of the colloidal particles, and the extent of critical, long-range correlations, which is measured by the correlation length ξ. In addition there are two time scales to be distinguished: the relaxation time of microstructure of extent R_V, which is characterized by the single-particle diffusion coefficient D_0, and the relaxation time of the microstructure of extent ξ, which is characterized by an effective diffusion coefficient $D^{\rm eff}(k=0)$. Two Péclet numbers should therefore be distinguished: the bare Péclet number Pe^0, which measures the amount of distortion of the microstructure over distances at most equal to the range R_V of the pair-interaction potential, and the dressed Péclet number λ, which relates to the amount of distortion over distances comparable to the correlation length ξ of the unsheared system. These two Péclet numbers are equal to

$$\mathrm{Pe}^0=\frac{\dot\gamma R_V^2}{2D_0}, \tag{1}$$

$$\lambda=\frac{\dot\gamma\xi^2}{2D^{\rm eff}(k=0)}. \tag{2}$$

[In Refs. [17,18] the parameter λ is defined as $(R_V^2/\beta\Sigma)\mathrm{Pe}^0(\xi/R_V)^4$. Some rearrangement with the help of Eqs. (3) and (4) below shows that this is precisely the same as the dressed Péclet number in Eq. (2). We should also mention that in Refs. [16,17] a third, dressed Péclet number Pe is introduced. The physically relevant dressed Péclet number, however, is the parameter λ.] The diffusion coefficient $D^{\rm eff}(k=0)$ is an effective diffusion coefficient that governs the diffusive behavior of colloidal particles over distances of the order ξ in systems in the vicinity of the critical point. The wave-vector-dependent effective diffusion coefficient is equal to

$$D^{\rm eff}(k)=D_0\beta\left[\frac{d\Pi}{d\bar\rho}+\Sigma k^2\right], \tag{3}$$

where Π is the osmotic pressure, $\bar\rho=N/V$ is the number density of colloidal particles, and Σ is a constant related to the square-gradient Cahn-Hilliard coefficient (which measures the contribution of gradients in the density to the local Helmholtz free energy). The correlation length of the unsheared system is related to $d\Pi/d\bar\rho$ and Σ as

$$\xi=\sqrt{\frac{\Sigma}{d\Pi/d\bar\rho}}. \tag{4}$$

Notice that since $\beta d\Pi/d\bar\rho\to 0$ on approach of the critical point, $D^{\rm eff}(k=0)\ll D_0$, that is, diffusive motion near the critical point becomes very slow. This is a phenomenon that is usually referred to as ''critical slowing down.'' Furthermore, $\xi\gg R_V$, so that $\lambda\gg\mathrm{Pe}^0$, that is, long-range critical correlations can be significantly distorted for shear rates where short-range correlations are hardly affected. When $\lambda<1$, long-range correlations are only slightly affected. Long-range correlations are severely affected only when $\lambda>1$. Similarly, short-range correlations are only affected when $\mathrm{Pe}^0>1$. One can therefore generally distinguish between three shear-rate regimes

$$\begin{aligned}
&\lambda<1, \quad \mathrm{Pe}^0\ll 1 \qquad \text{(the weak-shear regime)},\\
&\lambda>1, \quad \mathrm{Pe}^0\ll 1 \qquad \text{(the strong-shear regime)},\\
&\lambda>1, \quad \mathrm{Pe}^0\not\ll 1 \quad \text{(the very-strong-shear regime)},
\end{aligned} \tag{5}$$

The theoretical predictions in Refs. [17,18] are valid only in the weak- and strong-shear regimes since there the distortion of short-range correlations, measured by the bare Péclet number Pe^0, are neglected. For those shear-rate regimes the static structure factor $S^{\rm stat}$ under stationary shear flow is found to be given by

$$S^{\rm stat}(\mathbf{K})=S^{\rm eq}(K)+\frac{[S^{\rm eq}(K)-1]}{\lambda K_1}\times\int_{K_2}^{\pm\infty}dX(K^2-K_2^2+X^2)(K_2^2-X^2)\exp\left\{-\frac{F(\mathbf{K}|X)}{\lambda K_1}\right\}, \tag{6}$$

where $\mathbf{K}=\mathbf{k}\xi$ is a dimensionless wave vector with components K_j. The upper bound of the integral is $+\infty$ $(-\infty)$ when $K_1>0$ $(K_1<0)$. The function $F(\mathbf{K}|X)$ is a polynomial of the components of the dimensionless wave vector and X,

$$F(\mathbf{K}|X)=(X-K_2)(K^2-K_2^2)(1+K^2-K_2^2) + \tfrac{1}{3}(X^3-K_2^3)(1+2K^2-2K_2^2)+\tfrac{1}{5}(X^5-K_2^5). \tag{7}$$

The equilibrium structure factor S^{eq} is the Ornstein-Zernike structure factor

$$S^{\mathrm{eq}}(K)=\frac{1}{\beta\Sigma}\ \frac{1}{\xi^{-2}+k^2}=\frac{\xi^2}{\beta\Sigma}\frac{1}{1+K^2}. \tag{8}$$

This is the structure factor of the unsheared, quiescent system with correlation length ξ. Besides being valid only in the weak- and strong-shear regimes, the result (6) and (7) for the structure factor under stationary shear flow is also valid only in the mean-field region. In its derivation in Refs. [17,18] the equation of motion for the total correlation function h (the Fourier transform of which is essentially the structure factor) is linearized with respect to h. This is allowed for the small, critical wave vectors of interest near the critical point, since $h(\mathbf{r})\to 0$ for $r\to\infty$. The asymptotic solution of the equation of motion for large distances can thus be obtained by linearization with respect to h. What goes wrong on linearization very close to the critical point is the following. On linearization, terms of order h^2 are neglected with respect to linear terms in h. An important linear term is multiplied by $\beta d\Pi/d\overline{\rho}$. The actual assumption is thus that $(\beta d\Pi/d\overline{\rho})h \ll h^2$ for typical values that h attains due to the development of long-range correlations, that is, for $r\gg R_V$. Very close to the critical point, however, $\beta d\Pi/d\overline{\rho}$ becomes very small and the quadratic terms in h (and possibly even higher-order terms) are just as important as the linear term mentioned. Therefore, nonlinear equations of motion should be considered beyond the mean-field region. The result in Eqs. (6) and (7) obtained after linearization becomes less accurate on very close approach of the critical point. A third approximation that has been made to arrive at the result in Eqs. (6) and (7) for the structure factor is that hydrodynamic interactions between the colloidal particles are neglected.

The expressions (6) and (7) for the structure factor under stationary shear flow are easily evaluated numerically and some results are shown in Fig. 1. As can be seen from this figure, long-range correlations are diminished in all directions by the shear flow, except in directions where the component of the wave vector along the flow direction vanishes, $K_1=0$. That the structure factor is unaffected by shear flow in these directions can immediately be seen from Eq. (6) since there the shear rate $\dot\gamma\sim\lambda$ is always multiplied by K_1 and of course $S^{\mathrm{stat}}=S^{\mathrm{eq}}$ when $\lambda=0$. Hence

$$S^{\mathrm{stat}}(\mathbf{K})=S^{\mathrm{eq}}(K) \quad \text{for } K_1=0. \tag{9}$$

Identifying the integrand in Eq. (6) as a δ distribution for vanishing shear rates makes this statement mathematically rigorous (see Refs. [17,18]).

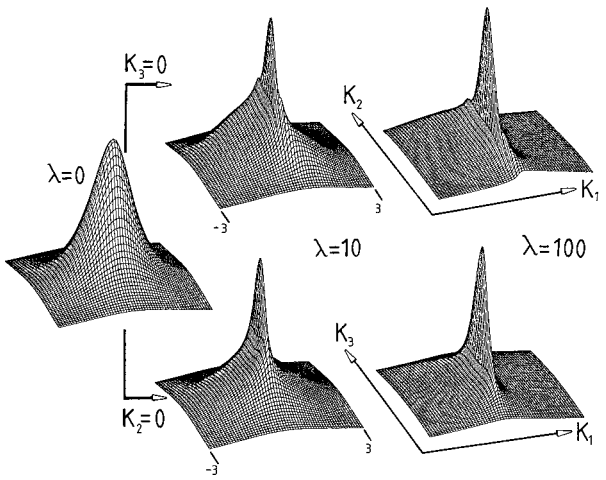

FIG. 1. Stationary structure factor $S^{\mathrm{stat}}(\mathbf{K})$ according to Eqs. (6) and (7) in the flow-gradient plane (upper figures) and the flow-vorticity plane (lower figures), for various values of the dressed Péclet number λ. The leftmost figure is the equilibrium, unsheared structure factor in Eq. (8), the Ornstein-Zernike structure factor.

To summarize, the result in Eqs. (6) and (7) for the structure factor under stationary shear flow is only valid (i) when $\mathrm{Pe}^0\ll 1$, that is, not in the very-strong-shear rate regime; (ii) in the mean-field region where linearization of equations of motion for the total-correlation function is allowed, not beyond mean field, where nonlinear equations of motion must be considered; and (iii) when hydrodynamic interactions are negligible.

The dressed Péclet number λ is the same as the dimensionless constant $\dot\gamma\tau_c$ mentioned in the Introduction in connection with earlier work. This can be seen as follows. The typical relaxation time τ_c of density waves with wavelength 2ξ is equal to $\tau_c=\xi^2/D^{\mathrm{eff}}(k=2\pi/2\xi)=\xi^2/2CD^{\mathrm{eff}}(k=0)$, with $C=\frac{1}{2}(1+\pi^2)$ a numerical constant. Here we used Eq. (4) for the correlation length. Hence $\dot\gamma\tau_c=\dot\gamma\xi^2/2D^{\mathrm{eff}}(k=0)$, which is precisely λ, apart from the numerical constant C. The shear-rate dependence of the wave vector k_c, for which shear effects on the structure factor becomes significant, as mentioned in the Introduction, can be obtained as follows. The Péclet number Pe_c that measures distortions of correlations extending over distances $2\pi/k_c$ is equal to $(2\pi/k_c)^2\dot\gamma/2D^{\mathrm{eff}}(k_c)$. Very close to the critical point, where $\beta d\Pi/d\overline{\rho}\approx 0$, we have, according to Eq. (3), $D^{\mathrm{eff}}(k_c)\sim k_c^2$ and hence $\mathrm{Pe}_c\sim\dot\gamma k_c^{-4}$. The distortion of the structure factor for wave vectors equal to k_c becomes significant when $\mathrm{Pe}_c\approx 1$ and hence $k_c\sim\dot\gamma^{1/4}$. Further away from the critical point we have $D^{\mathrm{eff}}(k_c)\approx D_0\beta d\Pi/d\overline{\rho}=\mathrm{const}$, so that it follows similarly that $k_c\sim\dot\gamma^{1/2}$. The exponent 1/4 found in this way should not be taken too seriously since the theory described above applies only to the mean-field region. The mean-field exponent of 1/2 found here is the rigorous mean-field exponent that expresses the shear-rate dependence of k_c (except that hydrodynamic interactions between the colloidal particles are neglected). The exponent beyond the mean field of 1/3 found for molecular systems by Onuki, Yamazaki, and Kawasaki [7] is in between our mean-field exponent 1/2 and our estimate of the exponent beyond mean field 1/4.

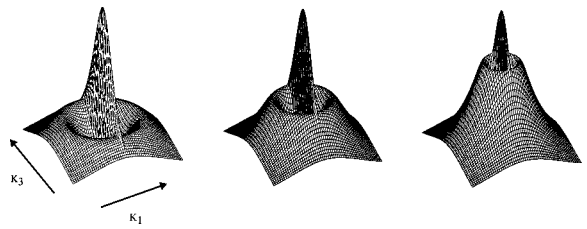

FIG. 2. Transient structure factors $S(\mathbf{K},t)$ in the flow-vorticity plane after cessation of shear flow, according to Eq. (11).

B. Relaxation after cessation of shear flow

After cessation of shear flow, the structure factor will change in time from its form under stationary shear flow to the Ornstein-Zernike equilibrium form. Under the same conditions for the validity of Eqs. (6) and (7) for the stationary sheared structure factor, the transient structure factors $S(\mathbf{K},t)$ obey the equation of motion [18]

$$\frac{\partial S(\mathbf{k},t)}{\partial t} = -2D^{\mathrm{eff}}(k)k^2[S(\mathbf{k},t)-S^{\mathrm{eq}}(k)], \qquad (10)$$

where the effective diffusion coefficient is given in Eq. (3). There is thus a ''driving force'' equal to the difference $S-S^{\mathrm{eq}}$ between the actual structure factor and its final equilibrium form and there is a rate limiting diffusion coefficient. The solution of Eq. (10) is easily found to be equal to

$$\begin{aligned} S(\mathbf{K},t) &= S^{\mathrm{eq}}(k)+[S^{\mathrm{stat}}(\mathbf{k})-S^{\mathrm{eq}}(k)] \\ &\quad \times \exp\{-2D^{\mathrm{eff}}(k)k^2t\} \\ &= S^{\mathrm{eq}}(K)+[S^{\mathrm{stat}}(\mathbf{K})-S^{\mathrm{eq}}(K)] \\ &\quad \times \exp\{-K^2(1+K^2)\,\dot\gamma t/\lambda\}, \end{aligned} \qquad (11)$$

where $\mathbf{K}$ is, as before, the dimensionless wave vector $\mathbf{K}=\mathbf{k}\xi$, with ξ the correlation length of the unsheared, equilibrium system. Here we used that $2D^{\mathrm{eff}}(k)k^2t=K^2(1+K^2)\,\dot\gamma t/\lambda$. This result predicts that at any time during relaxation, the structure factor takes its equilibrium form in directions perpendicular to the flow direction, that is, for $K_1=0$, just like the structure factor under stationary shear flow,

$$S(\mathbf{K},t)=S^{\mathrm{eq}}(K) \quad \text{for } K_1=0. \qquad (12)$$

Numerical results for transient structure factors during relaxation in the flow-vorticity plane are given in Fig. 2. As can be seen from this figure, a scattering ring develops that encloses the Ornstein-Zernike equilibrium structure factor at $K_1=0$, and the ring moves inward as time proceeds. After relaxation the structure factor attains its isotropic equilibrium Ornstein-Zernike form $S^{\mathrm{eq}}(K)$ for all wave vectors.

Notice that the result (11) for the transient structure factor predicts single exponential relaxation in time, which was also observed by Beysens, Gbadamassi, and Moncef-Bouanz [2] for binary fluids. Furthermore, relaxation times are only shear dependent through the shear rate dependence of the stationary sheared structure factor S^{stat} in the exponential prefactor. The argument of the exponent in Eq. (11) is independent of the shear rate since $\lambda\sim\dot\gamma$.

What is the origin of the scattering ring? As explained above, there is a driving force $S-S^{\mathrm{eq}}$ for relaxation that increases with decreasing wave vector (except in directions where $K_1=0$). This driving force gives rise to slower relaxation at larger wave vectors. The rate of relaxation is diffusion limited, as signified by the factor $D^{\mathrm{eff}}(k)k^2$ in Eq. (10). This diffusion rate gives rise to faster relaxation at larger wave vectors. The interplay between these two relaxation rate determining factors gives rise to an optimum relaxation rate at some intermediate wave vector, as a result of which the scattering ring appears.

A similar scattering ring is seen during spinodal decomposition, but its origin is completely different. In the case of spinodal decomposition one has a negative value of $d\Pi/d\overline{\rho}$, giving rise to an optimum value of the diffusion rate $D^{\mathrm{eff}}(k)k^2$ itself, as can be seen from Eq. (3) for the effective diffusion coefficient. In the present case the diffusion rate is a monotonically increasing function of the wave vector since $d\Pi/d\overline{\rho}>0$. It is the combination of the wave-vector dependence of the driving force and the diffusion rate that gives rise to an optimum relaxation rate. Notice also that in the case of spinodal decomposition the equilibrium state is a demixed state of two coexisting phases, while in the present case the equilibrium state is a homogeneous, one-phase state.

C. Shear-induced shift of the critical point

So far we have not addressed the shear-induced displacement of the critical point, a shift which may be of importance for data interpretation. It can be rigorously shown that the shear-induced shift of the critical point is related to the distortion of short-range correlations [19]. The displacement of the critical point is thus a function of the bare Péclet number Pe^0, not of the dressed Péclet number λ. In the weak- and strong-shear regime, as defined in Eq. (5), the displacement of the critical point is therefore negligible. There is a significant displacement only in the very-strong-shear regime, where Pe^0 is not very small. However, on very close approach of the critical point, a very small displacement may already be of importance. When the small distance to the critical point is of the same order as its small displacement, that displacement does have a significant effect. The theoretical results discussed in Secs. II A and II B are valid only in the mean-field region, relatively far away from the critical point, and only in the weak- and strong-shear regime. For the experimental verification of these theoretical results, the shear-induced shift of the critical point is therefore irrelevant. The shift may be relevant to some of the experiments that we will present here, which are performed extremely close to the critical point. To quantitatively interpret such experiments beyond the mean-field region, one should not only consider nonlinear equations of motion for the total correlation function, but also include distortions of short-range correlations, even for small values of the bare Péclet number.

Notice that in the mean-field region there is a significant distortion of the structure factor in directions perpendicular to the flow direction only when there is also a significant shift of the critical point. Both the shift of the critical point

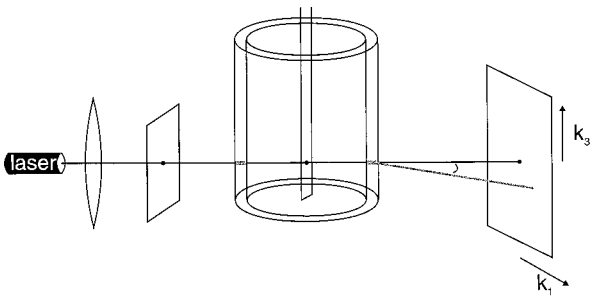

FIG. 3. Schematic of the experimental setup. See the main text for further details.

and distortions along directions where $k_1=0$ are significant in the mean-field region only when the bare Péclet number is not very small, that is, only in the very-strong-shear regime.

III. EXPERIMENT

A. Colloidal system

A relatively easy way to prepare a model colloidal system exhibiting a gas-liquid critical point is by mixing colloidal particles and polymer. In case the solvent is chosen such that the colloidal particles behave as hard spheres (in the absence of polymer) and is a θ solvent for the polymer, while the polymer does not adsorb onto the colloidal particles, approximate theories predict a gas-liquid phase transition when the size ratio of the colloidal particles to that of the polymer is less than about 0.3 [20]. The mechanism that leads to the effective attraction between the monodisperse colloidal particles that is necessary for a gas-liquid phase transition is easily understood: When two colloidal particles approach each other, there exists a region between these particles that is depleted from polymers, giving rise to an uncompensated osmotic pressure that drives the colloidal particles together. These attractive pair interactions between the colloidal particles are therefore commonly referred to as ''depletion-induced attractions'' [21,22].

The colloidal particles we used as spherical, amorphous silica particles, synthesized according to Stöber, Fink, and Bohn [23] and coated with stearyl alcohol according to van Helden, Jansen, and Vrij [24]. The radius of the coated silica particles in cyclohexane, as determined with dynamic light scattering, is 57 nm. In cyclohexane these particles behave like hard spheres. The polymer that is added is polydimethylsiloxane with a molecular weight of 204*k* and a radius of gyration in cyclohexane of 23 nm. The critical composition of this system is 101 g of silica particles and 1 g of polymer. The distance to the critical point is changed by adding or evaporating solvent. The critical polymer concentration is approximately 4 g/l, with a colloid volume fraction of about 25%.

B. Experimental setup

A schematic of the experimental setup is given in Fig. 3. The light source is a 5-mW He-Ne laser (Hughes, model 3225H-PC, wavelength 632.8 nm). A lense and a pinhole are used to control the primary beam. The shear cell is an optical Couette geometry, with an inner optical glass cylinder with diameter of 43.05 mm and a gap width of 1.90 mm. The entire Couette cell is placed in a toluene bath that serves both for thermostating at (25.0 ± 0.1) °C and for optical matching. Within the hollow rotation inner cylinder, filled with toluene, a stationary pinhole is placed to prevent detection of scattered light from the first gap. The second gap is arranged to be in the center of the cylindrical toluene bath. The scattered intensity is projected onto a translucent screen, from which the intensity is recorded by a computer-interfaced charge coupled device camera (EDC-1000, Electrim Corporation, 192×165 pixels, with eight-bit resolution). The beam is allowed to pass through a circular hole in the screen to prevent detection of radiation from the incident beam as well as light that is scattered by dust particles, which are inevitably present to some extent. The setup allows measurements in the scattering angle range of 1.2°–10°, corresponding to a wave-vector range of $(3\times10^5)-(3\times10^6)$ m^{-1}. In this wave-vector range the form factor of the colloidal particles is essentially equal to 1, so that the measured scattered intensity is directly proportional to the structure factor. Furthermore, we found the scattering of the polymers completely negligible compared to that of the colloidal silica particles.

C. Scattering under stationary shear flow

In this subsection we consider two concentrations: a concentration where the correlation length is equal to 850 ± 50 nm, referred to as system *A*, and a concentration where the correlation length is equal to 2.8 ± 0.5 μm, referred to as system *B*. Since the range of the pair-interaction potential is about 160 nm, being the sum of the diameter of a silica particle and that of a polymer, system *A* is not extremely close to the critical point (probably in the mean-field region), contrary to system *B*. These correlation lengths are measured by light scattering from the unsheared systems, using the Ornstein-Zernike (OZ) structure factor in Eq. (8): A plot of the reciprocal intensity against the square of the wave vector (referred to as OZ plots) yields the square of the reciprocal correlation length as the ratio of its intercept and slope. Figures 4(a) and 4(b) show the scattered intensities of the unsheared systems *A* and *B*, respectively. The OZ plots are shown in the insets, while the main figures show the structure factor as a function of the wave vector, with the solid line corresponding to the linear fit of the OZ plot. The data points are obtained as radially averaged intensities, after correction for refraction of scattered light by the glass cylindrical wall of the thermostating bath. As can be seen from Fig. 4, the structure factor of both systems *A* and *B* is well described by the Ornstein-Zernike form (8).

Figures 5(a) and 5(b) show the structure factor as a function of k_3 at $k_1=0$ for systems *A* and *B*, respectively, for several shear rates. As can be seen, there is almost no observable decrease of the structure factor for the mean-field system *A* up to the highest shear rate ($\dot\gamma=9.5$ s^{-1}), while for the system beyond the mean field, system *B*, even for the lowest shear rate ($\dot\gamma=0.1$ s^{-1}) there is already a significant distortion. The mean-field result (6) and (7) predicts that there should be no distortion in the directions where $k_1=0$, whenever the bare Péclet number $\mathrm{Pe}^0\ll1$. For system *A*, the highest shear rate corresponds to a bare Péclet number of 0.03 and the experimental observations in Fig. 5(a) sustain this mean-field prediction. For system *B*, however, the small-

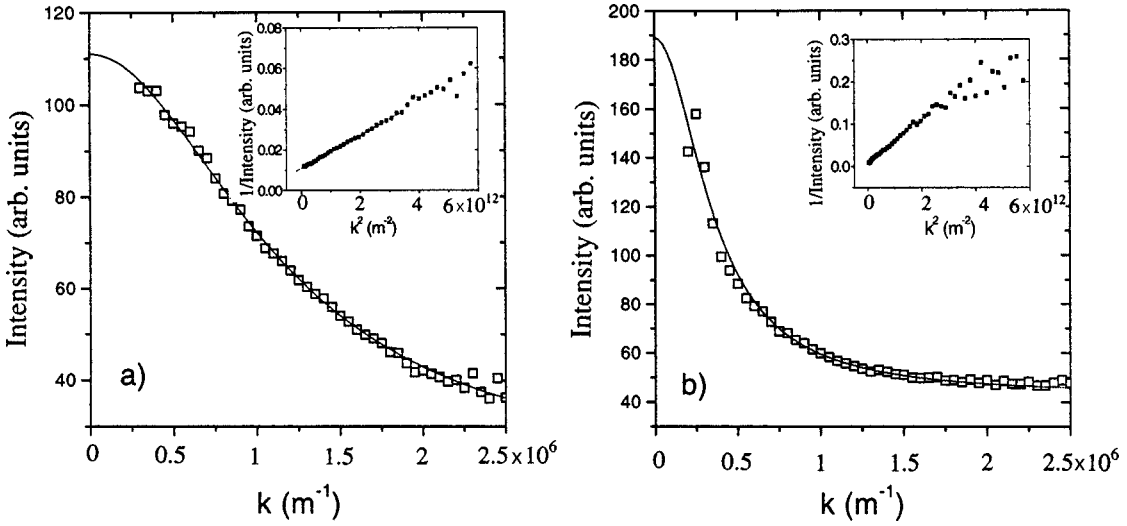

FIG. 4. Radially averaged intensities plotted versus the wave vector for (a) system *A* and (b) system *B*. The insets are OZ plots for the determination of the correlation length. The solid lines in the main figures are the best fits to the OZ plots.

est shear rate corresponds to a bare Péclet number as small as 0.0003, but still a significant distortion is found, even though $k_1=0$. There is thus a significantly different behavior very close to the critical point as compared to the mean-field behavior of the distorted structure factor.

In Figs. 6(a) and 6(b) the structure factor is plotted as a function of k_1 at $k_3=0$ for systems *A* and *B*, respectively, for the same shear rate range as in Figs. 5(a) and 5(b). A strong reduction of the structure factor of system *A* is found beyond $\dot{\gamma}=0.2\ \mathrm{s}^{-1}$, showing that the experiments relate to the strong-shear regime, where $\lambda>1$ [see the definition (5)]. The distortion of system *B* is even more pronounced than for system *A*. The same features are found for the structure factor as a function of k_1 at a finite value $7.2\times10^5\ \mathrm{m}^{-1}$ of k_3, as shown in Figs. 7(a) and 7(b). The data given in Figs. 6(a) and 7(a) are too noisy to allow for a quantitative test of the prediction (6) and (7) for the stationary sheared structure factor.

To summarize, we found that there is a pronounced shear-induced distortion of the structure factor in directions perpendicular to the flow (where $k_1=0$) in the strong-shear regime [as defined in Eq. (5)] very close to the critical point. There is no significant distortion in these directions for systems in the mean-field region, further away from the critical point, in accordance with the theoretical prediction (6) and (7) pertaining to the weak- and strong-shear regime.

D. Relaxation of the structure factor

After cessation of shear flow, the structure factor will evolve from its form under stationary shear flow to the equilibrium Ornstein-Zernike form. We performed light scattering experiments on a system very close to the critical point, beyond the mean-field region. The OZ plot for the unsheared system is given in the insert in Fig. 8(a), while the main figure gives the structure factor as a function of the wave vector, where the solid line is the Ornstein-Zernike structure factor (8) that follows from a fit of the OZ plot (see the discussion at the beginning of Sec. III C). The correlation

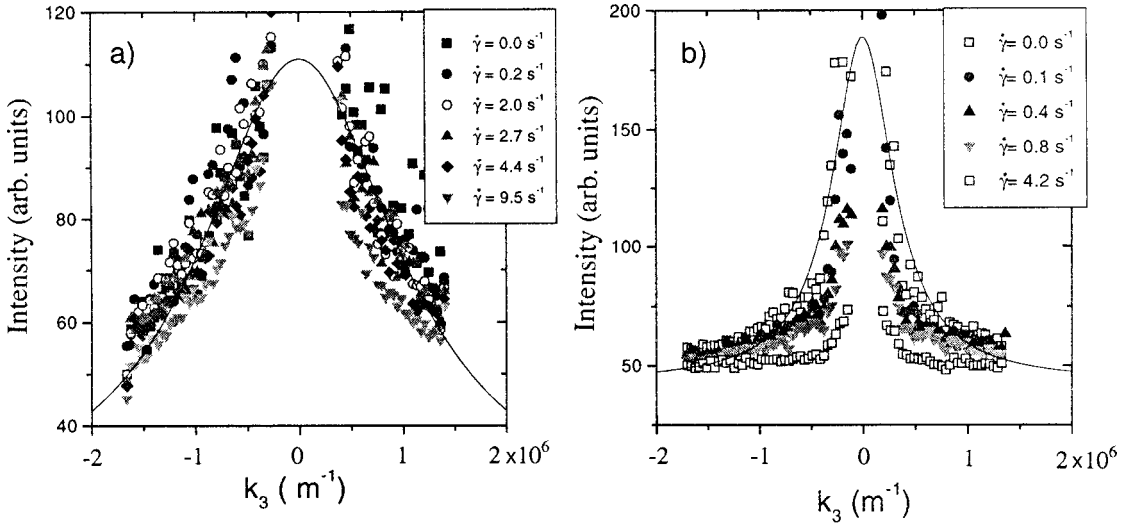

FIG. 5. Structure factor at $k_1=0$ as a function of k_3 for (a) system *A* and (b) system *B* for various shear rates as indicated in the figures. The solid lines are the Ornstein-Zernike structure factors as determined from the OZ plots in Figs. 4(a) and 4(b).

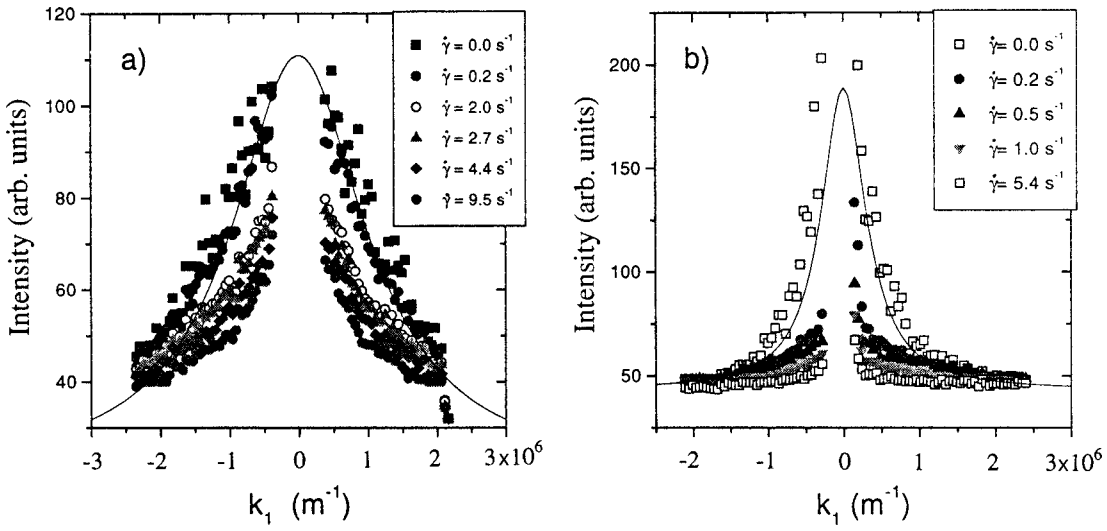

FIG. 6. Structure factor at $k_3=0$ as a function of k_1 for (a) system *A* and (b) system *B* for various shear rates as indicated in the figures. The solid lines are the Ornstein-Zernike structure factors as determined from the OZ plots in Figs. 4(a) and 4(b).

length that is found from the OZ plot is 2.6 ± 0.5 μm. The transient intensities after cessation of the shear flow with a shear rate equal to 100 s^{-1} are shown in Fig. 9. As can be seen, a scattering ring develops. We found that, except for a narrow region around $k_1=0$, the scattering patterns are circular symmetric to within experimental error [such a symmetry is also predicted by Eqs. (6) and (7) to within 1% in case of large λ's]. Radial averages, where the mentioned narrow region around $k_1=0$ is omitted, are given in Fig. 8(b) for several times after cessation of the flow. This figure reveals more clearly the formation of a peak in the structure factor, like in the theoretical mean-field results in Fig. 2. As discussed in Sec. III C the structure factor is severely distorted in directions where $k_1=0$ on very close approach of the critical point. What is missing in the experimental intensities in Fig. 9 as compared to the theoretical results in Fig. 2 is therefore the bright streak in the direction where $k_1=0$. Since there is as yet no theory available for the structure factor distortion beyond the mean-field region, the experimental results beyond the mean field in Fig. 8(b) are compared with the mean-field theoretical prediction in Eqs. (6), (7), and (11). The dashed lines in Fig. 8(b) represent the theoretical predictions for a dressed Péclet number equal to $\lambda=29\,000$. As can be seen, there is a semiquantitative agreement between the experiments and theory. The peak positions of the scattering maximima are well reproduced by theory. However, theory predicts a too fast growth for early times and a too slow growth for later times.

The effective diffusion coefficient $D^{\mathrm{eff}}(k)$ can be obtained, according to Eq. (11), by a single exponential fit of the time-dependent intensity at a fixed wave vector. This is done for three different wave vectors in Fig. 10. Single exponential fits are seen to overestimate the growth rate at early times, just as the fits in Fig. 8(b). From these single exponential fits we can estimate the effective diffusion coefficient, which is plotted in Fig. 11 as a function of the squared wave vector, which plot should be a straight line according to Eq. (3). This is indeed found to be the case, except for the

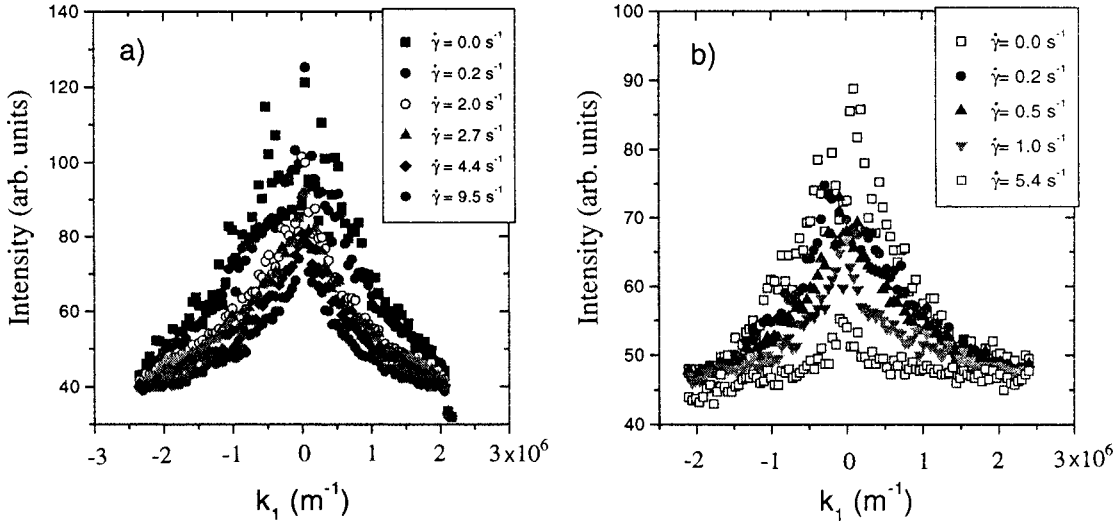

FIG. 7. Structure factor at $k_3=7.2\times10^5$ m^{-1} as a function of k_1 for (a) system *A* and (b) system *B* for various shear rates as indicated in the figures.

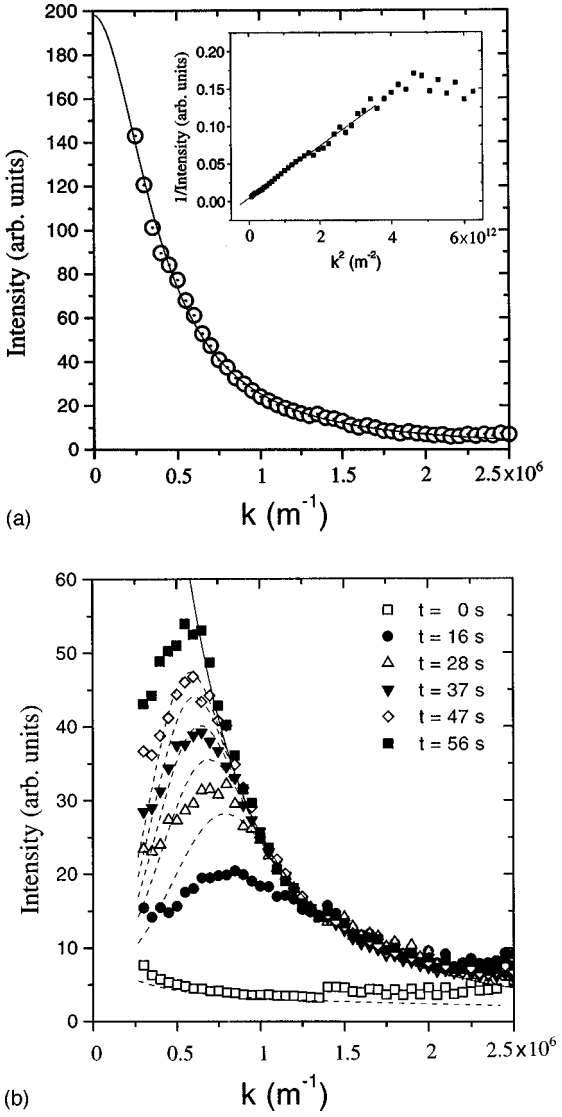

FIG. 8. (a) Radially averaged intensities as a function of the wave vector. The inset shows the OZ plot and the solid line in the main figure is the Ornstein-Zernike structure factor as determined from the OZ plot. (b) Radially averaged transient intensities after cessation of the shear flow with shear rate $\dot{\gamma}=100\ \mathrm{s}^{-1}$ as a function of the wave vector at various times as indicated in the figure. The solid line is the Ornstein-Zernike structure factor from (a) and the dashed lines are theoretical results from Eqs. (6) and (7) with $\lambda=29\,000$.

larger wave vectors where experimental uncertainties are large as the result of the small differences $S-S^{\mathrm{eq}}$ [see Fig. 8(b)]. Extrapolation to zero wave vector yields $D^{\mathrm{eff}}(k=0)=(2.5\pm0.5)\times10^{-14}\ \mathrm{m}^2\,\mathrm{s}^{-1}$, which is quite a bit smaller than the single-particle diffusion coefficient $D_0=4.3\times10^{-12}\ \mathrm{m}^2\,\mathrm{s}^{-1}$ for the colloidal silica particles in cyclohexane without polymer, signifying the pronounced critical slowing down. The dressed Péclet number λ, as defined in Eq. (2), is thus found to be in the range 7000–25 000, which is of the same order as we used to describe the relaxation data in Fig. 8(b). Of course these results must be considered as semiquantitative since we applied a mean-field result to interpret relaxation data for a system very close to the critical point. Values for $D^{\mathrm{eff}}(k=0)$ were obtained in the same way from relaxation data where the initial shear rates were 2.6 and 1.7 s^{-1}. We found the values $D^{\mathrm{eff}}(k=0)=(2.5\pm0.5)\times10^{-14}$ and $(3.5\pm0.8)\times10^{-14}\ \mathrm{m}^2\,\mathrm{s}^{-1}$, respectively. Since $D_{\mathrm{eff}}(k=0)$ is predicted to be independent of the shear rate, the three values we found should be the same. To within experimental errors this is indeed the case.

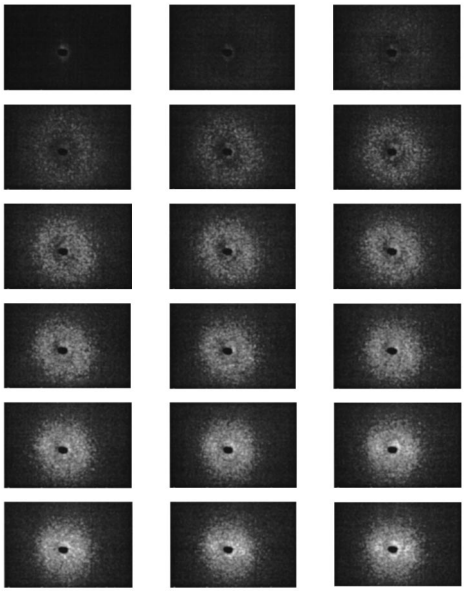

FIG. 9. Time series of scattering patterns during relaxation of the microstructure after cessation of a shear flow with shear rate 100 s^{-1}. The time between the subsequent images is about 4.5 s.

To summarize, we found experimentally transient structure factors during relaxation after cessation of shear flow that exhibit a peak, which means that there is an optimum relaxation rate at an intermediate wave vector. This is in accordance with mean-field theoretical predictions, where the scattering ring is shown to be the result of the interplay between a decreasing driving force and increasing diffusion rate with increasing wave vector. The agreement between mean-field theory and experiments very close to the critical

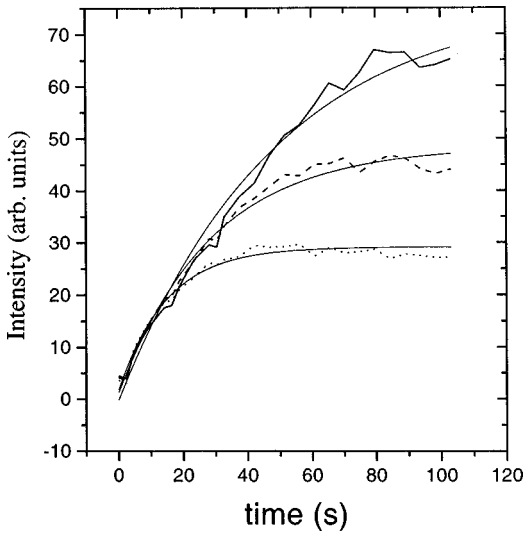

FIG. 10. Single exponential fits to Eq. (11) of the time-dependent intensity for three wave vectors ($k=0.60\times10^6\ \mathrm{m}^{-1}$, solid line; $k=0.75\times10^6\ \mathrm{m}^{-1}$, dashed line; $k=1.00\times10^6\ \mathrm{m}^{-1}$, dotted line).

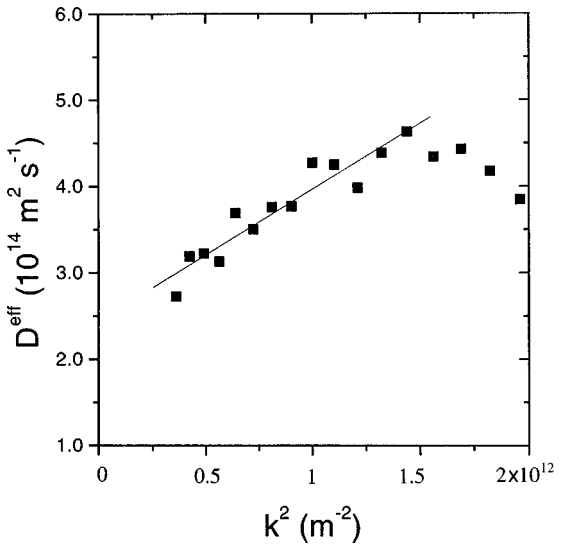

FIG. 11. Effective diffusion coefficient as a function of the squared wave vector.

point is semiquantitative. Further away from the critical point, ring formation is found experimentally to be less pronounced.

IV. SUMMARY AND CONCLUSIONS

Let us first summarize what the theory predicts.

(i) In the vicinity of the critical point there are two Péclet numbers to be distinguished: the dressed Péclet number λ and the bare Péclet number Pe^0 [see Eqs. (1) and (2)]. The dressed Péclet number measures the amount of shear-induced distortion of long-range critical microstructure, extending over distances of the order of the correlation length ξ, while the bare Péclet number measures the distortion of the short-range microstructure, extending over distances of at most the range R_V of the pair-interaction potential.

(ii) Three shear rate regimes are to be distinguished: the weak-, strong-, and very-strong-shear rate regimes [see the definition (5)]. In the weak-shear regime the long-range microstructure is only slightly affected by the shear flow ($\lambda < 1$). In the strong-shear regime the long-range microstructure is strongly affected, while short-range correlations are still essentially unaffected ($\lambda > 1$ and $\mathrm{Pe}^0 \ll 1$). In the very-strong-shear regime also short-range correlations are affected ($\mathrm{Pe}^0 \not\ll 1$).

(iii) The structure factor under stationary shear flow is highly anisotropic in the strong- and very-strong-shear regimes. There is no distortion perpendicular to the flow direction in the weak- and strong-shear regime. The distortion in these directions becomes significant only in the very-strong-shear regime.

(iv) During relaxation of the microstructure after cessation of the shear flow, there is an optimum growth rate at some intermediate wave vector, resulting in the development of a peak in the scattering pattern. This peak is the result of the interplay between a driving force and rate limiting diffusion, the former of which decreases and the latter increases relaxation rates on increasing the wave vector. In the weak- and strong-shear regimes the structure factor is equal to the equilibrium structure factor in directions perpendicular to the flow direction at all times.

(v) Relaxation after cessation of shear flow is predicted to be single exponential in time.

The above results are valid in the mean-field region, where equations of motion for the total correlation function can be linearized. In addition, effects of hydrodynamic interactions between the colloidal particles are assumed not to be essential.

As far as the shear-induced displacement of the critical point is concerned the predictions are the following.

(i) The shear-induced displacement of the critical point (and in fact of the entire spinodal) is related to distortion of short-range correlations and is therefore a function of the bare Péclet number. In the weak- and strong-shear regimes the displacement of the critical point is therefore negligible provided experiments are performed in the mean-field region. Very close to the critical point, a very small displacement of the critical point may be of importance when the small distance to the unsheared critical point is of the same order as its shear-induced displacement.

(ii) Distortions of the microstructure in directions perpendicular to the flow are always accompanied by a significant displacement of the critical point provided experiments are performed in the mean-field region. In the mean-field region both effects are significant only in the very-strong-shear regime.

Experimentally the following is found.

(i) In the mean-field region the shear-induced microstructure in directions perpendicular to the flow direction are not affected by shear flow in the weak- and strong-shear regimes, in accordance with theory.

(ii) Very close to the critical point, the microstructure is affected in directions perpendicular to the flow even in the strong-shear regime, contrary to mean-field results.

(iii) The formation of a peak in scattering patterns during relaxation of the microstructure after cessation of shear flow, which is predicted by mean-field theory, is indeed found experimentally. The ringlike transient scattering patterns are less pronounced further away from the critical point.

(iv) The agreement between mean-field predictions and experimental results very close to the critical point as far as the temporal evolution of the structure factor is concerned is semiquantitative. Contrary to mean-field theory, relaxation very close to the critical point deviates from single exponential temporal behavior. Mean-field theory overestimates relaxation rates at earlier times and underestimates relaxation times at later times.

Possible reasons for the different behavior of shear-induced distortions away from and very close to the critical point are, in order of what we feel is probable, as follows.

(i) Very close to the critical point nonlinear equations of motion for the total correlation function should be analyzed, contrary to the mean-field region, where linearization is allowed. Such nonlinear equations of motion will probably give rise to significant distortions perpendicular to the flow in the strong-shear regime and to nonsingle exponential temporal relaxation after cessation of shear flow.

(ii) It might be that hydrodynamic interactions between the colloidal particles are more important very close to the critical point.

(iii) The displacement of the critical point in the strong-shear regime may be significant very close to the critical point in case the distance to the unsheared critical point is of the same order as the very small shear-induced displacement.

The theoretical challenge is to analyze the nonlinear equations of motion of the total correlation function, to include long-range hydrodynamic interactions, and to include short-range distortions. These extensions of the mean-field theory, as described in Refs. [17,18], would elucidate the three above-mentioned points. The approach taken in Refs. [17,18] in principle allows one to systematically incorporate these extensions.

The things that remain to be done experimentally are a quantitative test of the prediction (6) and (7) for the structure factor under stationary shear in the mean-field region and further exploration of shear-induced distortions very close to the critical point. More accurate measurements than those presented in the present paper are required for this purpose.

[1] D. Beysens, M. Gbadamassi, and L. Boyer, Phys. Rev. Lett. **43**, 1253 (1979).
[2] D. Beysens, M. Gbadamassi, and B. Moncef-Bouanz, Phys. Rev. A **28**, 2491 (1983).
[3] A. I. Nakatani, H. Kim, Y. Takahashi, A. Takano, B. J. Bauer, and C. C. Han, J. Chem. Phys. **93**, 795 (1990).
[4] E. K. Hobbie, D. Hair, A. I. Nakatani, and C. C. Han, Phys. Rev. Lett. **69**, 1951 (1992).
[5] E. K. Hobbie, A. I. Nakatani, and C. C. Han, Mod. Phys. Lett. B **8**, 1143 (1994).
[6] E. K. Hobbie, A. I. Nakatani, Y. Yajima, J. Douglas, and C. C. Han, Phys. Rev. E **53**, R4322 (1996).
[7] A. Onuki, K. Yamazaki, and K. Kawasaki, Ann. Phys. (N.Y.) **131**, 217 (1981).
[8] X.-L. Wu, D. Pine, and P. Dixon, Phys. Rev. Lett. **66**, 2408 (1991).
[9] P. Dixon, D. Pine, and X.-L. Wu, Phys. Rev. Lett. **68**, 2239 (1992).
[10] J. W. van Egmond, D. E. Werner, and G. G. Fuller, J. Chem. Phys. **96**, 7742 (1992).
[11] H. Verduin and J. K. G. Dhont, Phys. Rev. E **52**, 1811 (1995).
[12] I. Bodnár and J. K. G. Dhont, Phys. Rev. Lett. **80**, 1662 (1998).
[13] A. Onuki, J. Phys.: Condens. Matter **9**, 6119 (1997).
[14] J. F. Schwarzl and S. Hess, Phys. Rev. A **33**, 4277 (1986).
[15] D. Ronis, Phys. Rev. A **29**, 1453 (1984).
[16] N. J. Wagner and W. B. Russel, Physica A **155**, 475 (1989).
[17] J. K. G. Dhont and H. Verduin, Physica A **235**, 87 (1997).
[18] J. K. G. Dhont and H. Verduin, J. Chem. Phys. **101**, 6193 (1994).
[19] J. K. G. Dhont, Phys. Rev. Lett. **76**, 4269 (1996).
[20] H. N. W. Lekkerkerker, W. C.-K. Poon, P. N. Pusey, A. Stroobants, and P. B. Warren, Europhys. Lett. **20**, 559 (1992).
[21] S. Asakura and F. Oosawa, J. Chem. Phys. **22**, 1255 (1954).
[22] A. Vrij, Pure Appl. Chem. **48**, 471 (1976).
[23] W. Stöber, A. Fink, and E. Bohn, J. Colloid Interface Sci. **26**, 62 (1968).
[24] A. K. van Helden, J. W. Jansen, and A. Vrij, J. Colloid Interface Sci. **81**, 354 (1981).